Supporting Information

Continuous synthesis of highly uniform noble metal nanoparticles over reduced graphene oxide using microreactor technology

Sha Tao[†,‡], Mei Yang[†,*], Huihui Chen[†,‡], Guangwen Chen[†,*]

† Dalian National Laboratory for Clean Energy, Dalian Institute of Chemical Physics, Chinese Academy of Sciences, Dalian, 116023, China

‡ University of Chinese Academy of Sciences, Beijing, 100049, China

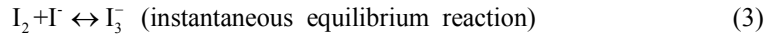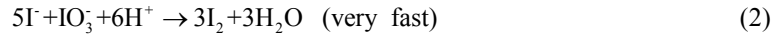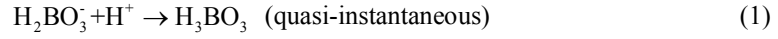The number of pages, figures and tables is 17, 11 and 4, respectively.

Corresponding authors

Mei Yang: +86-411-8437-9816 (phone), +86-411-8437-9327 (fax), yangmei@dicp.ac.cn (e-mail)

Guangwen Chen: +86-411-8437-9031 (phone), +86-411-8437-9327 (fax), gwchen@dicp.ac.cn (e-mail)

Quantitative analysis of mixing efficiency in the plugs

Villermaux/Dushman method on the basis of a parallel competing reaction system was employed to quantitatively analyze the mixing performance in the plugs at different process parameters:

$$H_2BO_3^- + H^+ \rightarrow H_3BO_3 \quad \text{(quasi-instantaneous)} \tag{1}$$

$$5I^- + IO_3^- + 6H^+ \rightarrow 3I_2 + 3H_2O \quad \text{(very fast)} \tag{2}$$

$$I_2 + I^- \leftrightarrow I_3^- \quad \text{(instantaneous equilibrium reaction)} \tag{3}$$

Reaction **1** is a quasi-instantaneous reaction, whereas Reaction **2** is fast but remarkably slower than Reaction **1**. Reaction **3** is an instantaneous equilibrium reaction. Aqueous solution A (0.020 M H_2SO_4) and aqueous solution B (0.25 M H_3BO_3+0.125 M NaOH+0.012 M KI+0.002 M KIO_3) were pumped into the cross-type micromixer with the same flow rate from inlet Ⅰ and Ⅲ, respectively. Octane was pumped into the cross-type micromixer from inlet Ⅱ. If the micromixing was ideal, aqueous solution A was instantaneously mixed with aqueous solution B, and H^+ ions were consumed by $H_2BO_3^-$ ions via Reaction **1**. Otherwise, H^+ ions were consumed competitively by Reaction **1** and **2**, and the formed I_2 further reacted with I^- ions to generate I_3^- ions according to Reaction **3**. The amount of I_3^- ions was determined by the mixing efficiency and could be measured by a UV-vis spectrophotometer (METASH UV8000) at 353 nm. The worse the mixing performance was, the larger the amount of I_3^- ions was. Segregating index (X_S) can be calculated from the amount of I_3^- ions:

$$X_S = \frac{Y}{Y_{ST}} \tag{4}$$

$$Y = \frac{2(V_1 + V_2)([I_2] + [I_3^-])}{V_1[H^+]_0} \tag{5}$$

$$Y_{ST} = \frac{6[IO_3^-]_0}{6[IO_3^-]_0 + [H_2BO_3^-]_0} \tag{6}$$

Y is the ratio of H^+ mole number consumed by Reaction **2** to the total H^+ mole number injected and Y_{ST} is the value of Y in the total segregation case when the micromixing process is infinitely slow.
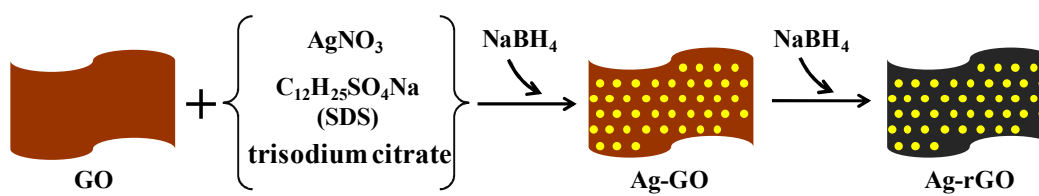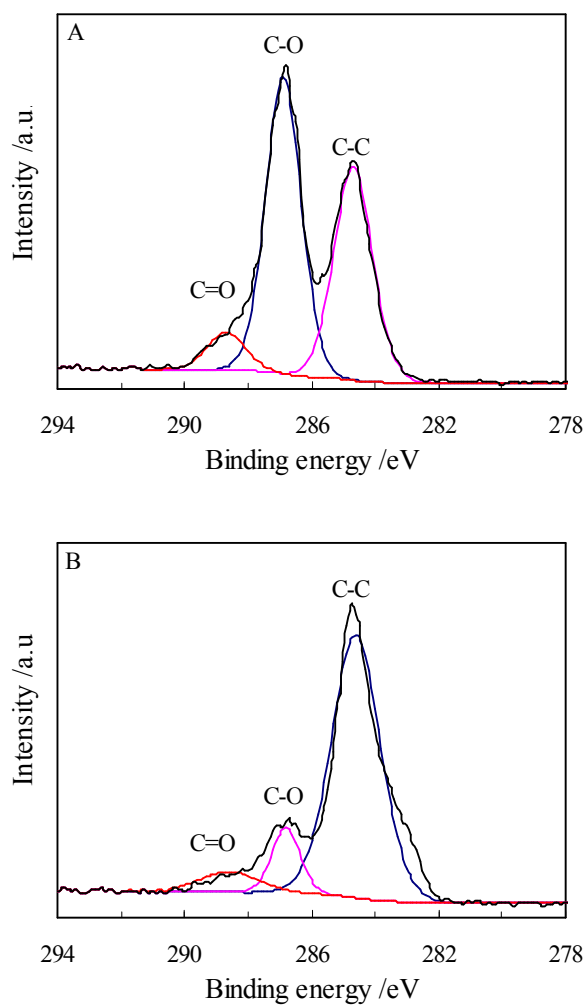
Figure S1. The schematic diagram of plausible formation mechanism of Ag-rGO composites.
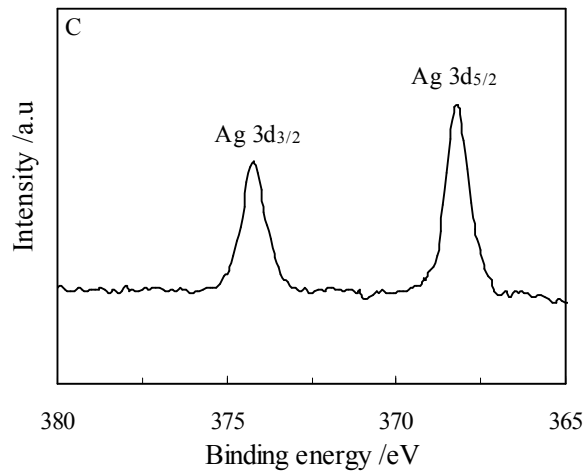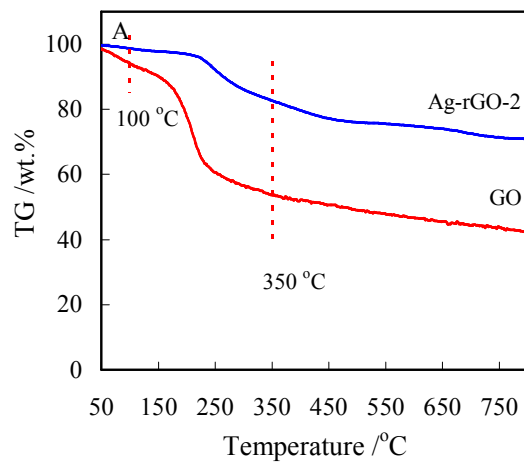
Figure S2. XPS spectra of (A) C 1s of GO (B) C 1s of Ag-rGO-S (C) Ag 3d of Ag-rGO-S.

Ag-rGO-S was synthesized under the condition of $Q_A=Q_B=0.2$ mL/min, $Q_{octane}=0.6$ mL/min, W/O ratio=2:3, $Q_{total}=1.0$ mL/min, $T=40$ °C, theoretical Ag weight percentage=21.3 wt.%, $\tau=1.38$ min.
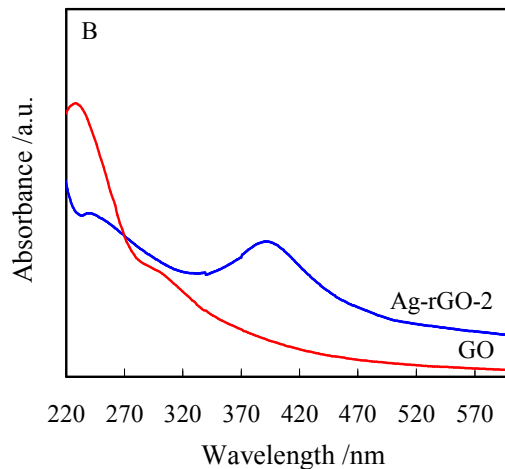
Figure S3. (A) TGA curves (B) UV-vis absorption spectra of GO and Ag-rGO-S. Ag-rGO-S was synthesized under the condition of $Q_A=Q_B=0.2$ mL/min, $Q_{octane}=0.6$ mL/min, W/O ratio=2:3, $Q_{total}=1.0$ mL/min, $T=40$ ^oC, theoretical Ag weight percentage=21.3 wt.%, $\tau=1.38$ min.
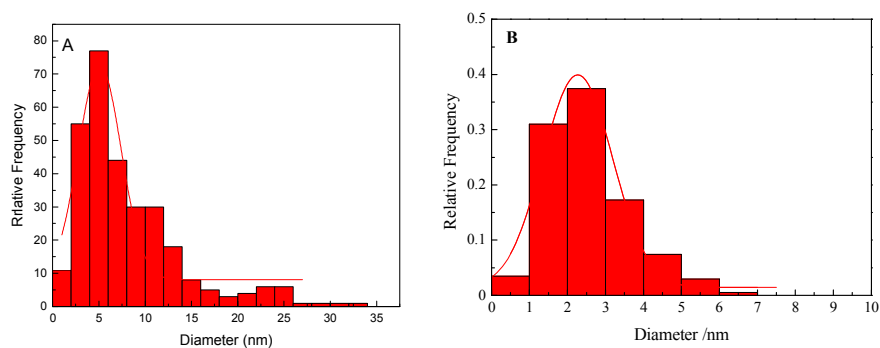

Figure S4. Particle size distribution of Ag NPs in (A) Ag-rGO-B (B) Ag-rGO-S. Ag-rGO-S was synthesized under the condition of $Q_A=Q_B=0.2$ mL/min, $Q_{octane}=0.6$ mL/min, W/O ratio=2:3, $Q_{total}=1.0$ mL/min, $T=40$ ^oC, theoretical Ag weight percentage=21.3 wt.%, $\tau=1.38$ min.

Figure S5. Particle size distribution of Ag NPs in Ag-rGO-S synthesized at different W/O ratios (A) W/O ratio=2:3, $Q_A=Q_B$=0.2 mL/min, Q_{octane}=0.6 mL/min, τ=1.38 min (B) W/O ratio=3:2, $Q_A=Q_B$=0.3 mL/min, Q_{octane}=0.4 mL/min, τ=1.36 min (C) W/O ratio=4:1, $Q_A=Q_B$=0.4 mL/min, Q_{octane}=0.2 mL/min, τ=1.35 min. Q_{total}=1.0 mL/min, T=40 ^{o}C, theoretical Ag weight percentage=21.3 wt.%.

Figure S6. Plug length and X_S as a function of (A) water/oil volume flow ratio (B) total volume flow rate.
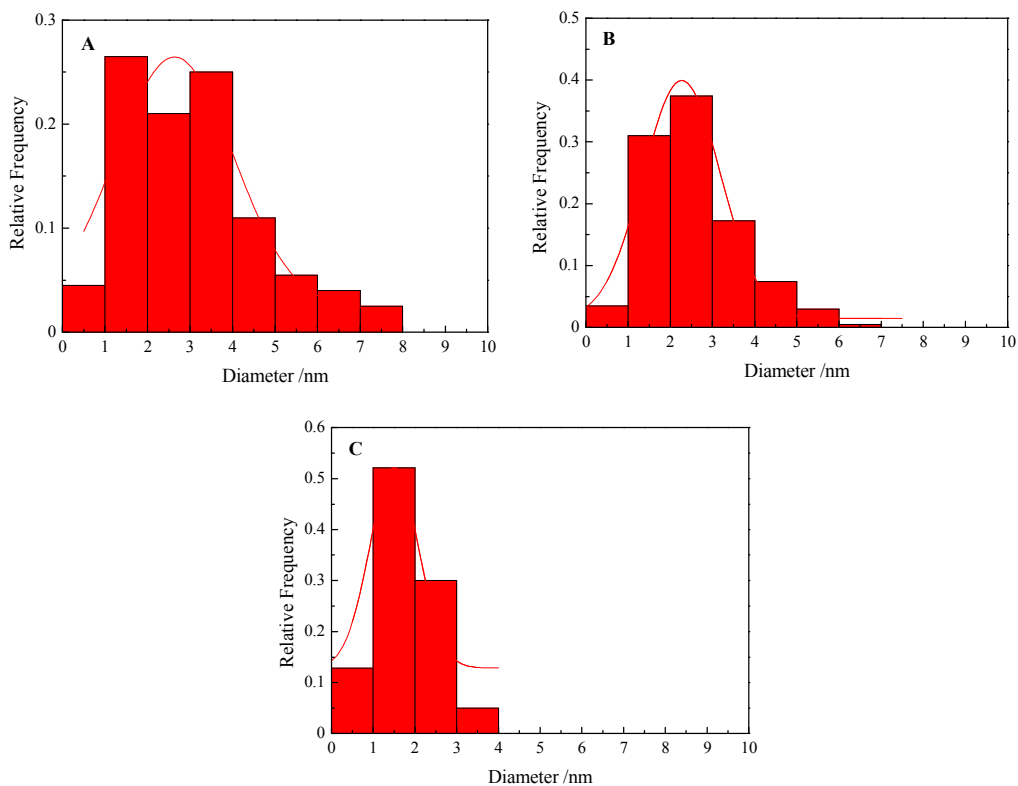
Figure S7. Particle size distribution of Ag NPs in Ag-rGO-S synthesized at different total volume flow rates (A) Q_{total}=0.5 mL/min, Q_A=Q_B=0.1 mL/min, Q_{octane}=0.3 mL/min, τ=2.76 min (B) Q_{total}=1.0 mL/min, Q_A=Q_B=0.2 mL/min, Q_{octane}=0.6 mL/min, τ=1.38 min (C) Q_{total}=1.5 mL/min, Q_A=Q_B=0.3 mL/min, Q_{octane}=0.9 mL/min, τ=0.92 min. W/O ratio=2:3, T=40 ^{o}C, theoretical Ag

weight percentage=21.3 wt.%.
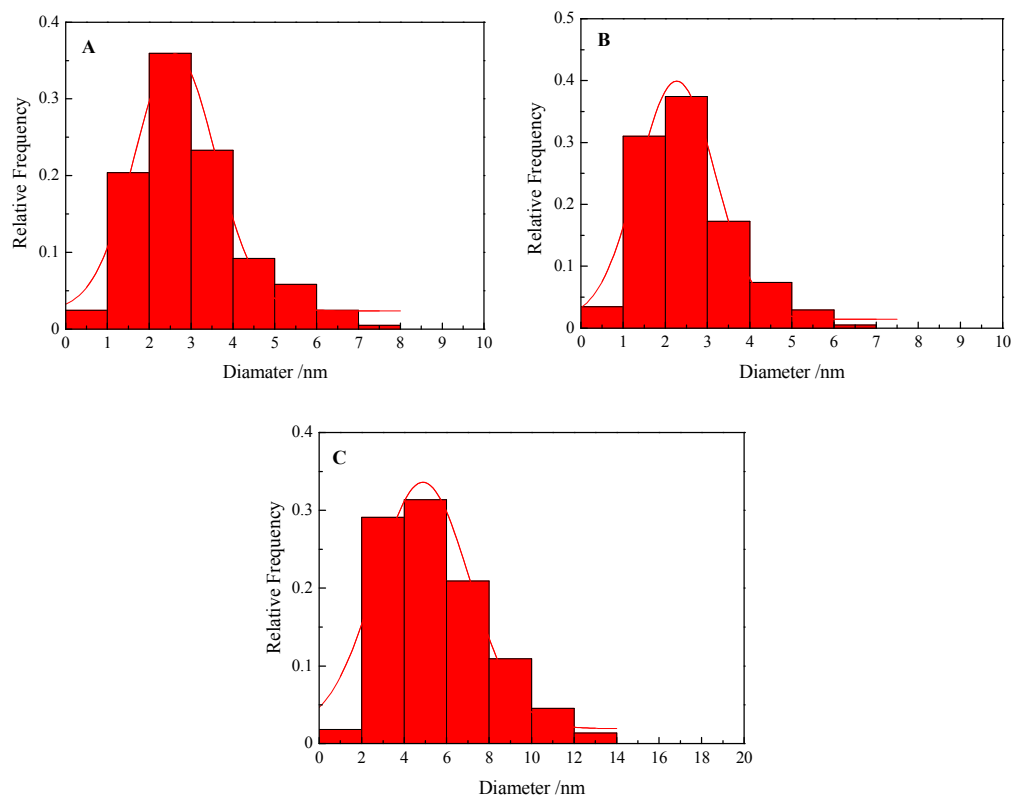
Figure S8. Particle size distribution of Ag NPs Ag-rGO-S synthesized at different synthetic temperatures (A) 20 $^{\circ}$C (B) 40 $^{\circ}$C (C) 60 $^{\circ}$C. Q_A=Q_B=0.2 mL/min, Q_{octane}=0.6 mL/min, W/O ratio=2:3, Q_{total}=1.0 mL/min, theoretical Ag weight percentage=21.3 wt.%, τ=1.38 min.
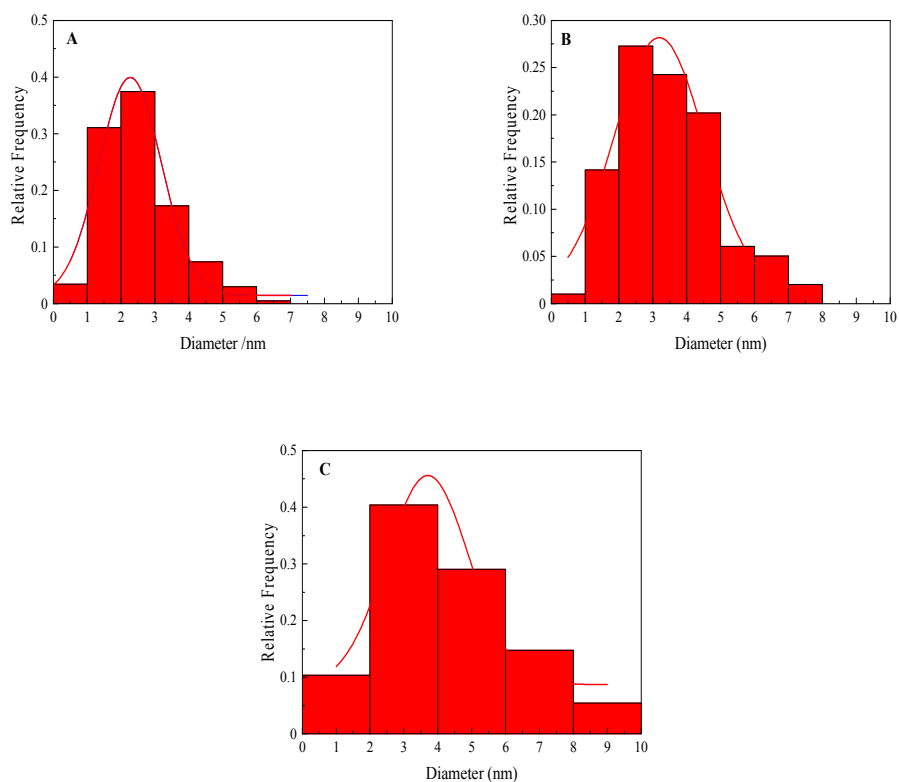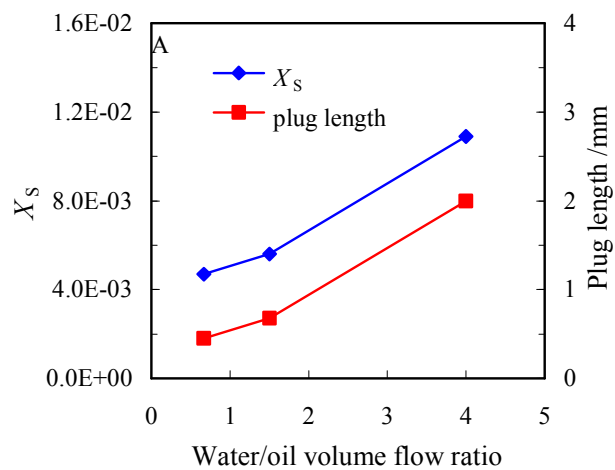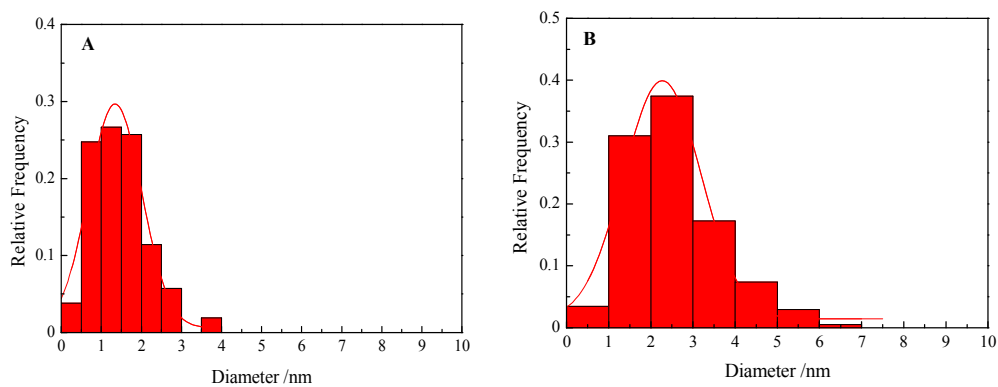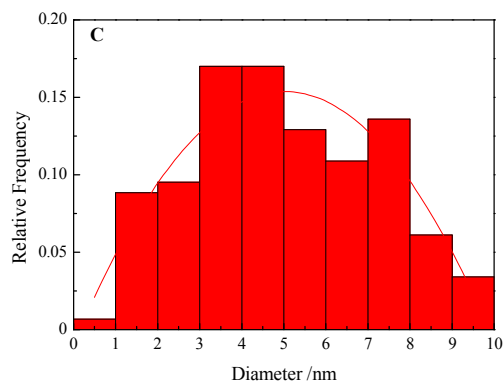
Figure S9. Particle size distribution of Ag NPs in Ag-rGO-S with different theoretical Ag weight percentages (A) 11.7 wt.% (B) 21.3 wt.% (C) 28.8 wt.%. $Q_A=Q_B$=0.2 mL/min, Q_{octane}=0.6 mL/min, W/O ratio=2:3, Q_{total}=1.0 mL/min, T=40 ^{o}C, τ=1.38 min.
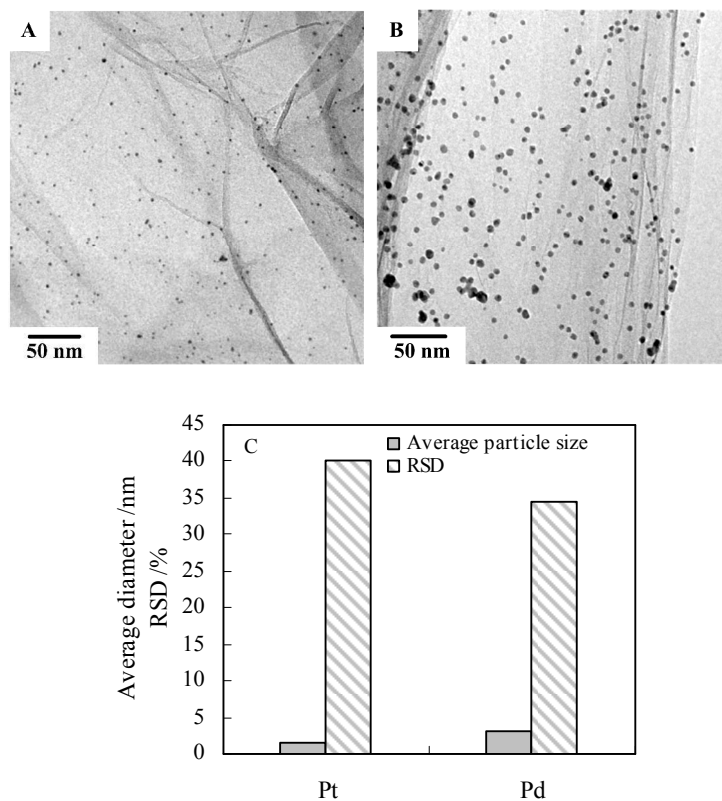
Figure S10. TEM images of (A) Pt-rGO-S (B) Pd-rGO-S; (C) average particle size and RSD of noble metal nanoparticles. $Q_A=Q_B$=0.2 mL/min, Q_{octane}=0.6 mL/min, W/O ratio=2:3, Q_{total}=1.0 mL/min, T=40 ^{o}C, theoretical Pt/Pd weight percentage=21.3 wt.%, τ=1.38 min.
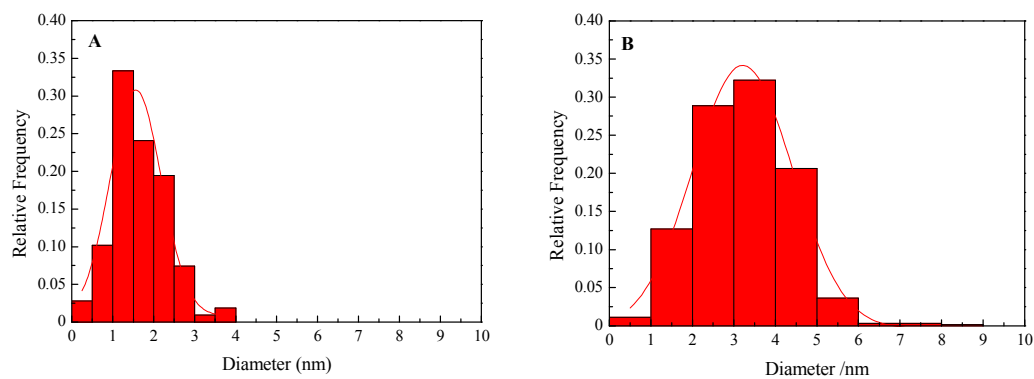
Figure S11. Particle size distribution of noble metal nanoparticles (A) Pt-rGO-S (B) Pd-rGO-S. Q_A=Q_B=0.2 mL/min, Q_{octane}=0.6 mL/min, W/O ratio=2:3, Q_{total}=1.0 mL/min, T=40 ^{o}C, theoretical Pt/Pd weight percentage=21.3 wt.%, τ=1.38 min.

Table S1A The materials and geometries of cross-type and T-type mixer.

Entry	Material[a]	Inlet channel					Outlet channel				
		Number	Cross section	I.D.[b]	O.D.[c]	L[d]	Number	Cross section	I.D.	O.D.	L
				mm	mm	cm			mm	mm	cm
Cross-type mixer	PTFE	3	Circular	0.6	1.6	1.0	1	Circular	0.6	1.6	1.0
T-type mixer	PTFE	2	Circular	0.6	1.6	1.0	1	Circular	0.6	1.6	1.0

Table S1B The material and geometries of capillary I and II.

Entry	Material	Cross section	I.D.	O.D.	L
			mm	mm	cm
Capillary 1	PFA	Circular	0.6	1.6	400.0
Capillary 2	PFA	Circular	0.6	1.6	100.0

[a] PTFE-polytetrafluoroethylene, PFA-polyfluoroalkoxy; [b] I.D.-inner diameter; [c] O.D.-outer diameter;

[d] L-length.

Table S2 The detailed experimental conditions predetermined in this work.

Sample	Variable	Stage 1					Stage 2	Synthetic temperature /°C	Theoretical noble metal weight percentage /wt.%	Residence time /min[b]
		Q_A /mL/min	Q_B mL/min	Q_{octane} mL/min	Water/oil volume flow ratio[a]	Total flow rate mL/min[a]	Q_C mL/min			
Ag-rGO	water/oil volume flow ratio	0.2	0.2	0.6	2:3	1.0	0.2	40	21.3	1.38
		0.3	0.3	0.4	3:2	1.0	0.3	40	21.3	1.36
		0.4	0.4	0.2	4:1	1.0	0.4	40	21.3	1.35
	total volume flow rate	0.1	0.1	0.3	2:3	0.5	0.1	40	21.3	2.76
		0.2	0.2	0.6	2:3	1.0	0.2	40	21.3	1.38
		0.3	0.3	0.9	2:3	1.5	0.3	40	21.3	0.92
	synthetic temperature	0.2	0.2	0.6	2:3	1.0	0.2	20	21.3	1.38
		0.2	0.2	0.6	2:3	1.0	0.2	40	21.3	1.38
		0.2	0.2	0.6	2:3	1.0	0.2	60	21.3	1.38
	Theoretical Ag weight percentage	0.2	0.2	0.6	2:3	1.0	0.2	40	11.7	1.38
		0.2	0.2	0.6	2:3	1.0	0.2	40	21.3	1.38
		0.2	0.2	0.6	2:3	1.0	0.2	40	28.8	1.38
Pt-rGO	-	0.2	0.2	0.6	2:3	1.0	0.2	40	21.3	1.38
Pd-rGO	-	0.2	0.2	0.6	2:3	1.0	0.2	40	21.3	1.38

[a] As the water/oil volume flow ratio and total volume flow rate in the first stage dramatically affected the average particle size and particle size distribution of Ag NPs in Ag-rGO-S, the water/oil volume flow ratio and total volume flow rate was calculated using the volume flow rates of solution A, B and octane in the first stage.

[b] The residence time was the average amount of time spent in the microchannel by the mixed solutions (stage 1: solution A + solution B + octane; stage 2: solution A + solution B + solution C + octane). The residence time was calculated by the following equation:

$$\tau = \frac{V_{\text{stage1}}}{Q_{\text{stage1}}} + \frac{V_{\text{stage2}}}{Q_{\text{stage2}}}$$

(7)

where τ represents the residence time; Vstage1 and Vstage2 represents the volume of microchannels used in stage 1 and 2; Qstage1 and Qstage2 represents the total volume flow rates of mixed solutions in stage 1 and 2, respectively.

$$V_{\text{stage1}} = V_{\text{cross-type, outlet}} + V_{\text{capillary I}} + V_{\text{T-type, inlet}}$$

(8)

$$V_{\text{stage2}} = V_{\text{T-type, outlet}} + V_{\text{capillary II}}$$

(9)

$$Q_{\text{stage1}} = Q_{\text{A}} + Q_{\text{B}} + Q_{\text{octane}}$$

(10)

$$Q_{\text{stage2}} = Q_{\text{A}} + Q_{\text{B}} + Q_{\text{octane}} + Q_{\text{C}}$$

(11)

where Vcross-type, outlet, Vcapillary I, VT-type, inlet, VT-type, outlet and Vcapillary Ⅱ is the volume of cross-type mixer's outlet channel, capillary Ⅰ, T-type mixer's inlet channel, T-type mixer's outlet channel and capillary Ⅱ; QA, QB, QC and Qoctane is the flow rate of solution A, B, C and octane. The residence time under different conditions was added into the revised manuscript.

Table S3 The space time yields (*STY*) of Ag-rGO composites synthesized in continuous mode and

batch mode.

Operation mode	$m_{Ag\text{-}rGO}$ /mg[a]	τ /min	V /mL	STY^{b} /g·h^{-1}·L^{-1}
continuous	0.07	1.38	1.42	2.15
batch	12.7	60	110[c]	0.12

[a] Ag theoretical weight percentages of Ag-rGO composites synthesized in continuous mode and batch mode were both 21.3%. The continuous mode was carried out under the experimental condition of Q_A=Q_B=0.2 mL/min, Q_{octane}=0.6 mL/min, synthetic temperature= 40 ^{o}C.

[b] The equation of the space time yield was defined as:

$$STY = \frac{m_{Ag\text{-}rGO}}{V\tau} \qquad (12)$$

where $m_{Ag\text{-}rGO}$, V and τ are the theoretical mass of Ag-rGO composite, volume of reaction occurring, and residence time, respectively.

[c] The final volume of mixed solution was used for the calculation of *STY*.

Table S4 The average particle sizes of Ag NPs in Ag-rGO nanocompoistes synthesized via

solution-phase reduction.

Sample	Ag precursor	Reducing agent	Solvent	Average particle size /nm	Ref.
Ag-rGO	Silica coated Ag NPs	Hydrazine hydrate	Water	~5 nm	1
Ag/rGO	$AgNO_3$	-	Water	~5 nm	2
AgNP-GO	$AgNO_3$	Vitamin C	Water	15-55 nm	3
Ag/rGO	$AgNO_3$	DMF	DMF	20-40 nm	4
Ag-rGO	$AgNO_3$	$NaBH_4$	Water	5-60 nm	5
AgNP-GE	$AgNO_3$	$NaBH_4$	Water	~10 nm	6

Ag/GN	AgNO$_3$	glucose	Supercritical CO$_2$	~5 nm	7
Ag-rGO	AgNO$_3$	Ethylene glycol	Water	~4.7 nm	8
Ag-rGO	AgNO$_3$	NaBH$_4$	Water	1.5-5.6 nm	This work

References

(1) Bhunia, S. K.; Jana, N. R. Reduced Graphene Oxide-Silver Nanoparticle Composite as Visible Light Photocatalyst for Degradation of Colorless Endocrine Disruptors. *ACS Appl. Mater. Inter.* **2014**, *6*, 20085-20092.

(2) Han, X. W.; Meng, X. Z.; Zhang, J.; Wang, J. X.; Huang, H. F.; Zeng, X. F.; Chen, J. F. Ultrafast Synthesis of Silver Nanoparticle Decorated Graphene Oxide by a Rotating Packed Bed Reactor. *Ind. Eng. Chem. Res.* **2016**, *55*, 11622-11630.

(3) Hui, K. S.; Hui, K. N.; Dinh, D. A.; Tsang, C. H.; Cho, Y. R.; Zhou, W.; Hong, X.; Chun, H. H. Green Synthesis of Dimension-Controlled Silver Nanoparticle-Graphene Oxide with in Situ Ultrasonication. *Acta Mater.* **2014**, *64*, 326-332.

(4) Dutta, S.; Ray, C.; Sarkar, S.; Pradhan, M.; Negishi, Y. T. P. Silver Nanoparticle Decorated Reduced Graphene Oxide (rGO) Nanosheet: A Platform for SERS Based Low-Level Detection of Uranyl Ion. *Appl. Mater. Inter.* **2013**, *5*, 8724-8732.

(5) Murphy, S.; Huang, L.; Kamat, P. V. Reduced Graphene Oxide-Silver Nanoparticle Composite as an Active SERS Material. *J. Phys. Chem. C* **2013**, *117*, 4740–4747.

(6) Zhou, Y.; Yang, J.; He, T.; Shi, H.; Cheng, X.; Lu, Y. Highly Stable and Dispersive Silver Nanoparticle-Graphene Composites by a Simple and Low-Energy-Consuming Approach and Their Antimicrobial Activity. *Small* **2013**, *9*, 3445-3454.

(7) Yuan, M.; Su, F.; Chen, Y. Supercriticalfluid Synthesis and Tribological Applications of Silver

Nanoparticle-Decorated Graphene in Engine Oil Nanofluid. *Sci. Rep-UK* **2016**, *6*, 31246.

(8) Kumar, S.; Selvaraj, C.; Scanlon, L. G.; Munichandraiah, N. Ag Nanoparticles-Anchored

Reduced Graphene Oxide Catalyst for Oxygen Electrode Reaction in Aqueous Electrolytes and also

a Non-Aqueous Electrolyte for Li-O$_2$ Cells *Phys. Chem. Chem. Phys.* **2014**, *16*, 22830-22840.